ISSN 8755-6839

SCIENCE OF TSUNAMI HAZARDS

Journal of Tsunami Society International

Volume 34 Number 3 2015

COASTAL RISK IN THE ALGIERS REGION (ALGERIA): INSIGHTS FROM TSUNAMI VELOCITIES, SEISMIC GROUND MOTION AND REMOTE SENSING

L. A. Amir[1,*], A. Dahlab[1], M.B. Douaifia[1]

[1] *USTHB-FSTGAT, Department of Geophysics, BP 32, 16111 Bab Ezzouar, Algiers, Algeria*

B. Theilen-Willige[2]

[2] *Institute of Applied Geosciences, Berlin University of Technology (TU Berlin), Berlin, Germany*

ABSTRACT

The Algiers region (Algeria) is exposed to destructive earthquakes that sometimes trigger tsunamis. In this paper, we present an interdisciplinary approach that identifies the locations prone to related induced damage for a worst-case scenario off Algiers. Firstly, a tsunami modeling for a 7.6 earthquake in the Khair Al Din Bank is computed with the Geoclaw package. The simulation indicates that the maximum values for the surface heights are about 1.5 meters and 40 to 60 m/s for the flow velocities. Seismic shaking maps are computed as well using the OpenSHA application for the same earthquake scenario. The results show that the peak ground accelerations and peak ground velocities are the highest in the Algiers massif, which means that this area is the most exposed to a high level of infrastructural damage. Finally, the use of remote sensing and GIS applications helped to generate a susceptibility to flooding hazard map for the bay of Algiers. This approach showed that the central and the eastern part of the bay have the higher susceptibility degree to flooding.

Key Words: *Tsunami, ground motion, Algeria, flow velocities, surface heights, Algiers.*

Vol. 34, No. 3, page 173 (2015)

1. INTRODUCTION

Tsunami hazard in the Algerian coast is related to earthquakes with epicenters located offshore the western Mediterranean margin or to slides due to the numerous canyons evidenced from geophysical marine surveys (Yelles-Chaouche, 1991; Domzig et al., 2006). Several coastal cities have been destroyed in the past by coastal and offshore earthquakes. Minor to moderate tsunamis occurred in the past and have been as well reported in numerous papers with information as for the extent of the coastal inundation induced or triggered observed sea-waves. A series of boulders have been found and measured in the Algerian coast from Tipaza to Dellys (Maouche et al., 2009). The transportation of these boulders suggests catastrophic events that hit the Algerian coast. Dating (Carbon 14) and sedimentary and morphological analysis of the boulders provided quantitative data as for (1) the potential source (historical and past earthquakes) and (2) the water height necessary to displace these marine deposits (Maouche et al., 2009). All the calculations used to evaluate the physics of boulder movement were based on Nott's equations that only focused on the wave heights. However, these equations have been revised and new hydrodynamic equations have been proposed and applied for boulder transport from the flow velocity (Nandasena et Tanaka, 2013).

Hydrodynamic equations for tsunami modeling are based on the mass and momentum conservation laws. Tsunami processes involve three main steps that are (1) the generation, (2) the propagation, (3) the shoaling on the coast usually with debris transportations. Water waves' amplitude depends on the bathymetry so that when reaching the coast, tsunami waves increase in height. When flooding the coast, the waves impact the roads, houses and carry debris with such strength that the assessment of tsunami hazard and risk has to be completed with data on the energy and the flow velocities.

In this paper, an interdisciplinary approach to evaluate the tsunami and the associated / related earthquake risk for the Algiers region is presented. The Algiers bay and the central part of Algeria are regularly marked by moderate shallow earthquakes. Located at the limit between the African and the European convergent plates, the earthquakes sometimes reach magnitude above 6 and trigger tsunami waves and turbidity currents. The second section of this paper presents the materials and methods used to evaluate the tsunami hazard from tsunami modeling for a structure identified by previous studies as a potential source for a major event off Algiers. The simulation output provides with surface heights and flow velocities for a series of points of interest in the studied area. A ground motion analysis (seismic) is also developed to discuss on the ratio tsunami versus earthquake risk. A remote sensing and a GIS application are as well included as a combined approach to investigate the exposure to flooding and risk for the studied region. The third section presents the results obtained. Finally, the fourth section discusses on the research output here investigated for coastal risk assessment and exposure related to vulnerability and susceptibility to flooding.

2. MATERIALS AND METHODS

2.1 The tsunamigenic scenario for Algiers

The highest seismogenic potential in the Algiers Bay is related to the Sahel Fold and anticline

(inland) and the Khayr al Din Bank (KDB) (offshore, in the Neogene margin) (Yelles et al., 2009; Heddar et al., 2012). In this study, the potential source for tsunami generation is considered to be associated to the co-seismic vertical uplift of the sea bottom in case of an important earthquake with an epicenter at the foot of the KDB where a reverse active fault has been identified and mapped from marine geophysical surveys (Domzig, et al., 2006; Yelles et al., 2009).

Due to the collision between the African and the European tectonic plates, the Algiers region is under a compressive regime with a stress field oriented NNW-SSE. The active structures mapped in the margin, off NW of Algiers, strike in the E-W and NNW-SSE directions. The strike angle varies between 60˚ to 70˚ (Domzig, et al., 2006; Yelles, et al., 2009). The MARADJA cruise provided accurate maps showing the margin's strike changes abruptly from the Algiers Massif with an E-W direction in the eastern part of the Massif and a NW-SE direction in the western part. Yelles et al. (2009) also indicated that from east near Tamentfoust to west near Ain Benian, the margin depicts first a roughly 60˚E and E-W direction. Active seismogenic structures in the Algiers region extend over 70 to 80 km in length (Domzig et al., 2006; Yelles, et al., 2009; Heddar et al., 2012). In particular, the KDB is about 80 km long in a W-E direction, from the front of the Algiers massif to the north west of Cherchell. It depicts an overall E-W direction with a major change in a NW-SE direction in its eastern tip off Ain Benian (Yelles et al., 2009).

Using the seismological empirical laws, a magnitude of 7.6 is expected in the region. The Khayr al Din fault-related fold located at the foot of the margin is a blind reverse fault dipping in the southward direction. The authors agree on considering a mean dip for the fault of 47 +/- 7˚ (Yelles et al., 2009). Length and width for the fault geometry can be estimated from empirical relationships. Consequently, in this work we assume a width of 29.3 km and a length of 73.3 km for the tsunami source. The epicenter is here located at 2.98E, 36.98N and the focal depth is 07 km. Finally, and the amount of slip in the program was suggested from past destructive earthquakes related to blind reverse faulting. In 1980, the El Asnam earthquake (Ms = 7.3) revealed the existence of a reverse blind fault and produced surface faulting in the Chelif basin (Yielding, 1985). The field studies carried out in the epicentral area identified three main thrust segments with distinct co-seismic slip values. Yielding (1985) reported the vertical displacement reached a maximum of about 5 m near the central part of the fault, though averaged about 2 – 3 m. This allows us to propose a mean value of 3.5 meters for the dislocation in the present study.

2.2 Methodology

2.2.1 The hydrodynamic modeling

Tsunami waves are long water waves with three distinct phases from the generation to the impact on shorelines. Tsunami waves' propagation is expressed using the conservation laws for mass and momentum. The shallow water equations solved by the Geoclaw package describe any of the diverse flow regimes from the global domain to more near field complex areas in the shoreline or onto dry land (George and Leveque, 2006). The set of equations include flows that defined a hyperbolic system for tsunami modeling. The Geoclaw package was developed to solve the integral conservation law for mass and momentum from a finite volume method based on the Riemann numerical solutions approach (George and Leveque, 2006). The set of equations include flows that defined a hyperbolic system for tsunami modeling. The Riemann solver for the tsunami

modeling can then be written by the equation hereby (eq.1) (George & Leveque, 2006):

$$\boldsymbol{q}t + A\,\boldsymbol{q}\boldsymbol{q}x = 0 \quad (eq.\ 1)$$

Where $\boldsymbol{q} = (h,\ hu\ ,12gh2+hu2,b)T$ and $A \in \mathbb{R}4*4$, h is the water depth, u is the horizontal velocity, g is the gravitational constant and b is the bottom surface elevation.

In this work, the manning coefficient was set to 0.025 for depths lower to zero and 0.06 for dry land modeling. The time step was 05 minutes and the duration of the modeling was set to 02 hours. The topography was extracted from the ETOPO 1 arc - minute custom grid data (Amante & Eakins, 2009). The grid extends from 0˚E to 8˚E for the longitude and 36˚N to 44˚ N for the latitude (Figure 1).

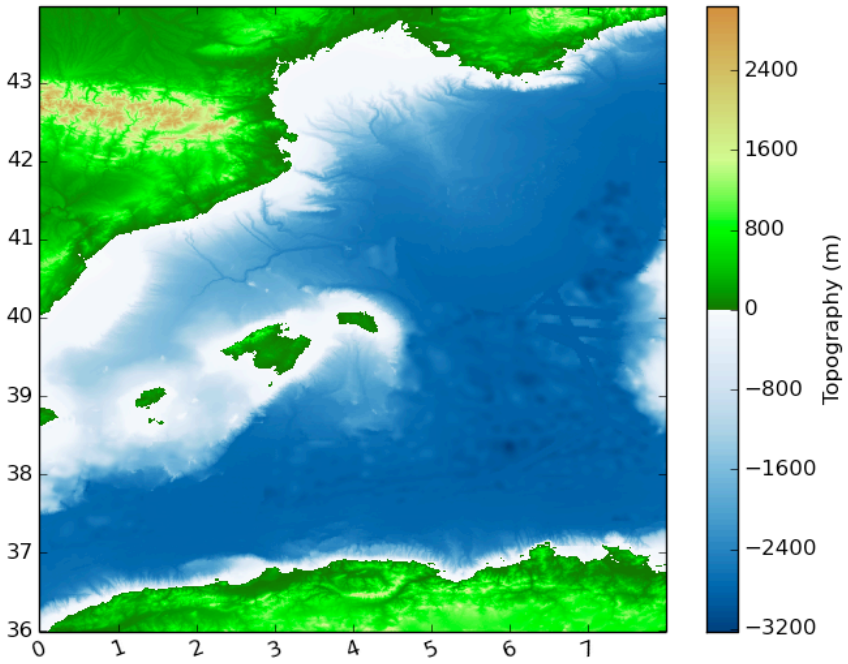

Figure 1: Topography of the West Mediterranean – source: ETOPO 1mn (NGDC-NOAA).

2.2.2 The ground motion

Earthquake damage can be evaluated through seismic hazard analysis and the modeling of the ground motion. Many studies on loss estimations for urban cities rely on the peak ground acceleration data provided either from seismic records or from numerical modeling (Field et al., 2005; Field et al., 2005). In this work, the interdisciplinary approach to evaluate the coastal risk for the Algiers region involves the presentation of the earthquake shaking maps computed from the OpenSHA application (Field et al., 2005).

Peak ground accelerations and peak ground velocities are estimated using an earthquake scenario and the appropriate attenuation law/relationships. The earthquake source introduced in the OpenSHA application can either be a fault segment or a single point representing the assumed

hypocenter. In this work, the Abrahmson and Silva attenuation law (Abrahamson et Silva, 1997) is selected. This relationship has been set up for a large series of earthquake around the world and therefore, is one of the most general attenuation laws. The earthquake source considered is one single point rupture. The hypocenter introduced in the model is the one considered for the tsunami modeling with the Geoclaw software. The seismological parameters introduced in the application are those considered for the tsunami modeling with the Geoclaw package.

2.2.3 Remote sensing for flooding hazard assessment

Airborne and space borne remote sensing systems and image analysis techniques have been developed to an extent where civil and commercial earth observation instruments can contribute significantly to supporting the management of major technical and natural disasters as well as humanitarian crisis situations. Open-source tools as OpenStreetMap or Google Earth were used for gaining the necessary information, as well as evaluations of classified satellite imageries and further Web-tools. GoogleEarth-data were evaluated in Quantum-GIS. Satellite data downloaded from the Global Land Cover Facility, University of Maryland and the EarthExplorer of the USGS / USA contributed to the geodatabase. A RapidEye-satellite imagery of Algiers was provided by BlackBridge, Berlin / Germany. Free Open Source Software (FOSS) such as LEOWorks provided by ESA and Quantum-GIS (GNU General Public License) were applied additionally to ArcGIS / ESRI and ENVI / EXELIS digital image processing software. This data mining is aiming at visualizing critical areas and providing information about damage in case of emergency due to flooding hazards as fast as possible, as the civil protection units need this information for their management. The almost actual inventory of land use and infrastructure (bridges, railroads, roads, river embankments, etc.), industrial facilities and the structure of settlements and cities (considering age, structure and function of buildings) is an important issue for the hazard assessment and damage loss estimation. Digital image processing using software was used not only for the enhancement of RGB-imageries, but also to derive water index (NDWI—Normalized Difference Water Index) and vegetation index (NDVI Normalized Difference Vegetation Index) images. Another important digital processing method applied in this study was the supervised and unsupervised image classification. In urban areas the inventory of building stocks, built-up density, building heights, infrastructure, or undeveloped areas is relevant to the vulnerability identification and quantification.

For the detection of water currents in the Bay of Algiers various image-processing procedures were tested and the results combined with available wind information. Evaluations of LANDSAT satellite imageries in time series contribute to a better knowledge of water current dynamics, influenced among other factors (wind direction and speed, etc.) by the coastal morphology.

Morphometric properties and disposition of coastal areas can influence to a great extent the susceptibility to flooding due to flash floods, storm surge, meteo- or tsunami waves The systematic inventory of morphometric properties according to a standardized GIS-approach based on digital elevation data and evaluations of satellite imageries from flooding prone areas contribute considerably to the detection of areas, that are more susceptible to flooding due to their geomorphologic disposition. It offers a low-cost to no-cost approach (as the used DEM data are free), that can be used in any area, providing a first basic data stock for emergency preparedness by providing susceptibility-to-flooding maps.

The term susceptibility does not predict when a hazard will occur. The susceptibility assessment derives places, which are exposed to flooding hazards due to their morphologic disposition. The factors influencing the flooding susceptibility are classified into causal and triggering. The causal factors determine the initial favorable conditions for the occurrence, while the triggering factors such as high precipitation rates or storm surge principally determine the timing. Causal factors are, among others, the slope gradient, curvature, lithology and groundwater table level. The triggering mechanisms are quite unpredictable, as they vary in time and their composition. The percentage of influence of one factor also changes in consideration of seasonal and climatic factors. In very hot and dry seasons the risk of flooding to flash floods is generally lower than in wet seasons with higher precipitation occurrence. Some of these causal factors can be integrated as layers into a GIS. Therefore, based on DEM data morphometric maps were created and terrain parameters were extracted such as shaded relief, aspect and slope degree, minimum and maximum curvature or plan convexity maps using ENVI and ArcGIS software as well as Quantum-GIS. The morphometric parameters such as lowest height level, lowest slope degree, amount of flow accumulation and minimum curvature provide information of the terrain inundation susceptibility.

3. RESULTS

3.1 The tsunami modeling for the KDB Scenario (Algiers region)

The tsunami modeling was computed from the Geoclaw package (George and Leveque, 2006). The code includes a subroutine that calculates the seafloor deformation using the Okada theory for a half-space (Okada, 1992). The results show that a single fault segment off North of Algiers (Length*Width = 73.3 km*29.9 km) with a slip of 3.5 meters produces a maximum seafloor uplift deformation of about 1.6 meters (Figure 2).

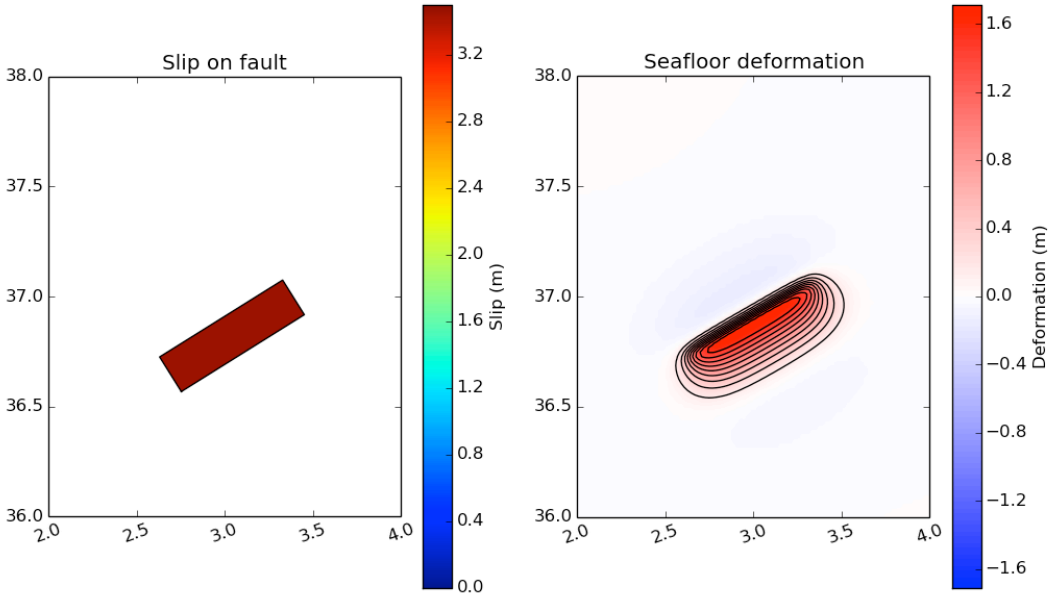

Figure 2: Co-seismic slip (meters) (2a) and Sea-bottom deformation (meters) (2b) (vertical uplift) simulated for a 7.6 magnitude earthquake, off Algiers

In this work, we present the surface height and the horizontal velocities simulated for a series of gauge/ points of interest located along the Algiers coast (see Table 1).

Table 1: Location of the points of interest for the Algiers region

ID Point of Interest	Latitude (˚N)	Longitude (˚E)
Gauge 1	1.48	36.53
Gauge 2	2.81	36.7
Gauge 3	3.1	36.95
Gauge 4	3.64	36.83
Gauge 5	3.1	36.85
Gauge 6	3.2	36.88

Figure 3 displays the tsunami propagation after five and ten minutes after the onset of the earthquake. The results show the immediate decrease of the sea in the central part of North Algeria. After five minutes, the surface heights here depicted reach above 1.5 meters in the Bou Ismail Bay and northward the epicentral zone (Figure 3a). The rising of the sea is as well shown for the gauges along the Algiers bay. Ten minutes after the onset of the earthquake, the water surface disturbance covers a larger area and water waves seemed to be trapped in both bays (rising / decrease, water flow) (Figure 3b).

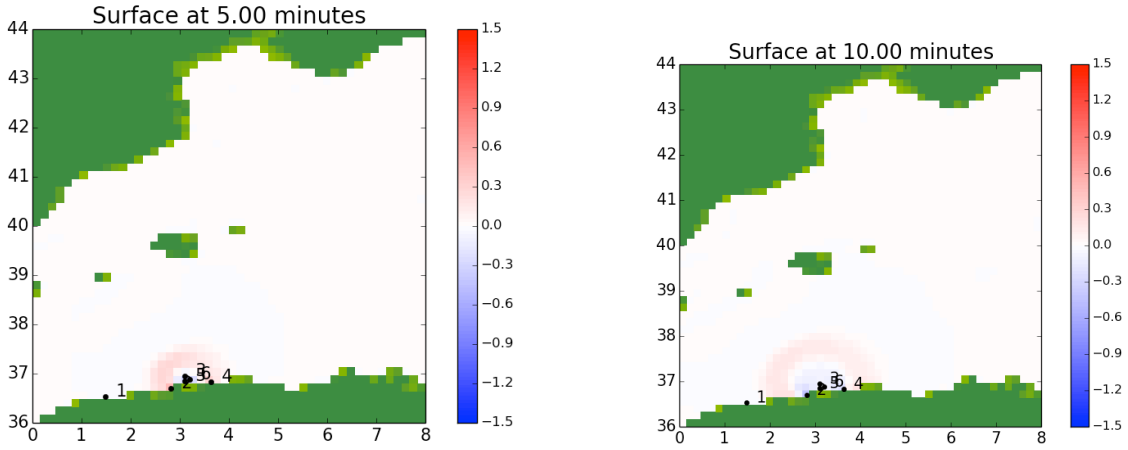

Figure 3: Tsunami propagation 05 minutes (3a) and 10 minutes (3b) after the onset of the earthquake.

The figure 4 presents the water heights simulated for the six gauges in the Algiers region. Water heights above one meter are obtained for gauge 2, 5 and 6. These three points of interests are located precisely nearby the epicenter. At gauge 1, the water height never exceeds 0.2 meters. At gauge 3, the instantaneous rising of the sea is as well simulated but is lower than what is observed closer the Algiers coast (0.8 meter). At gauge 4, the maximum water surface estimated is lower than 0.5 meter.

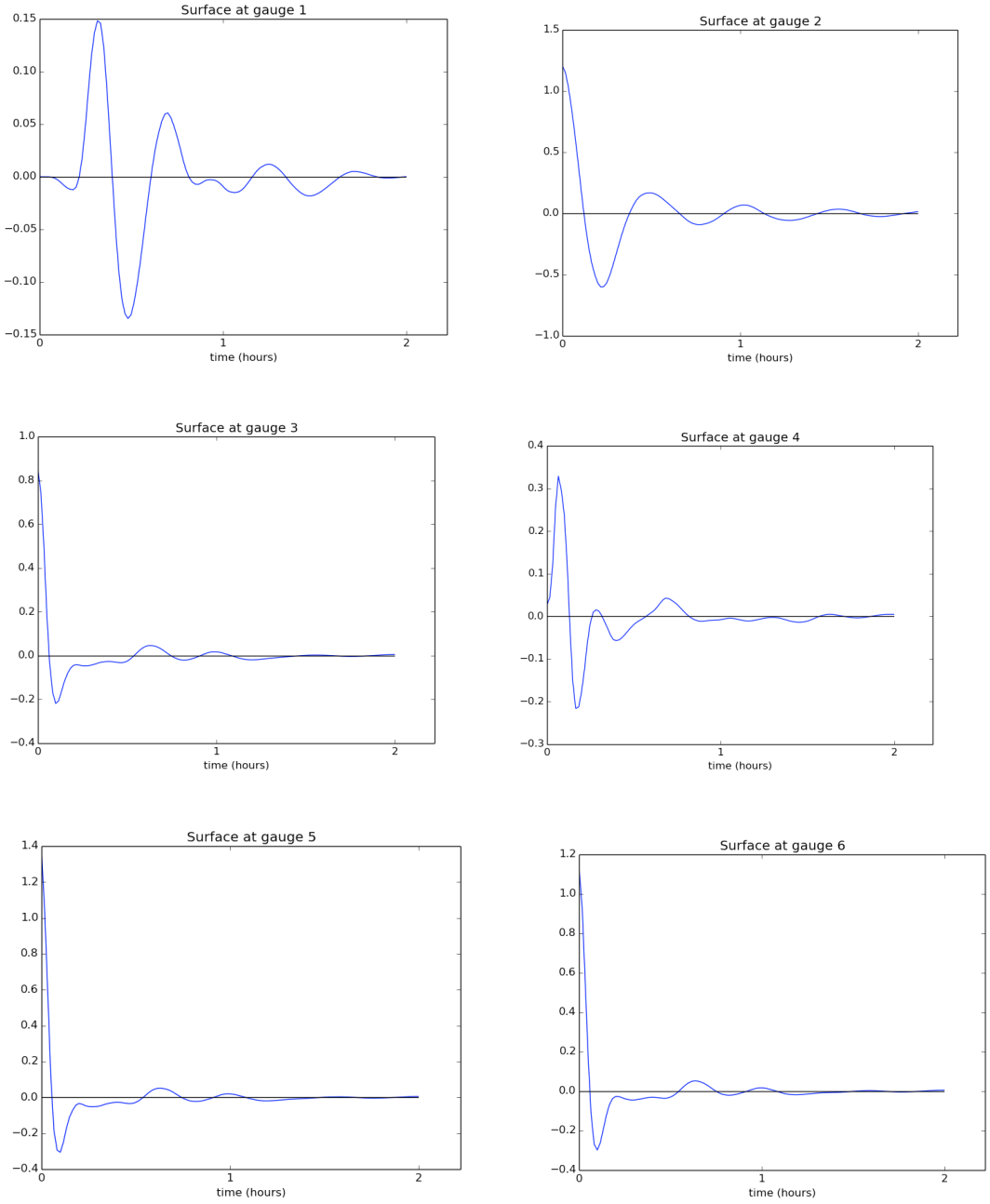

Figure 4: Water heights (meters) simulated with the GeoClaw package for the 6 points of interests in the Algiers region.

Figure 5 depicts the flow velocities computed for gauge 2, 3, 4, 5 and 6. Both horizontal velocities are here presented (m/s). The results show that the v component (Oy direction) is higher than the u component (Ox direction) for all the gauges. The highest value for the u component is obtained for the gauges 2 and 4. The maximum values are above 20 m/s. The highest value for the v component is obtained for gauge 3 with 60 m/s. The lowest value for the v component is for gauge 4. Comparable velocities are estimated for both gauges 5 and 6 with about 10 m/s for the u component and about 40 m/s for the v component.

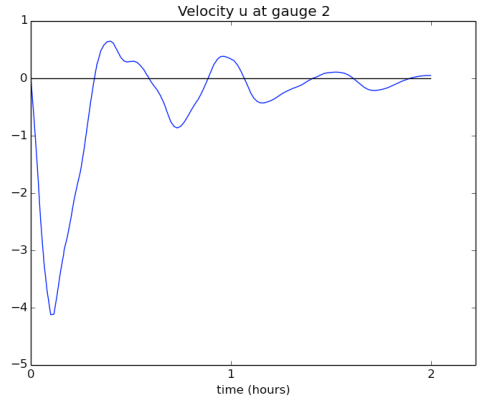
Velocity u at gauge 2
time (hours)

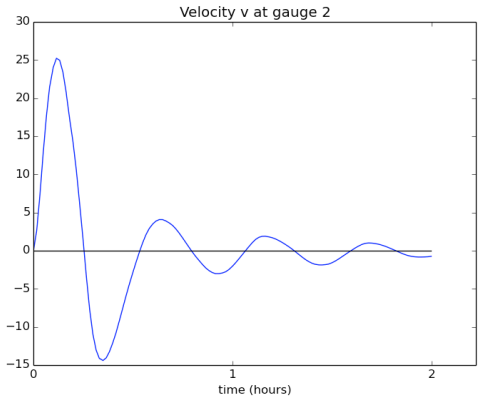
Velocity v at gauge 2
time (hours)

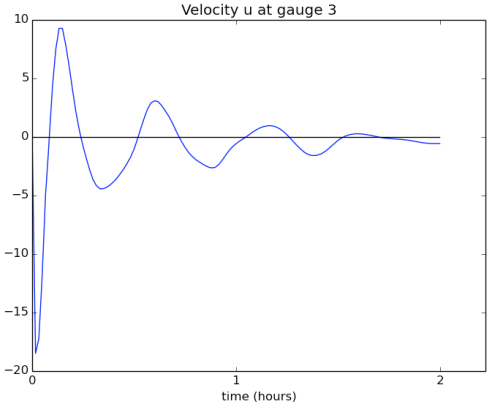
Velocity u at gauge 3
time (hours)

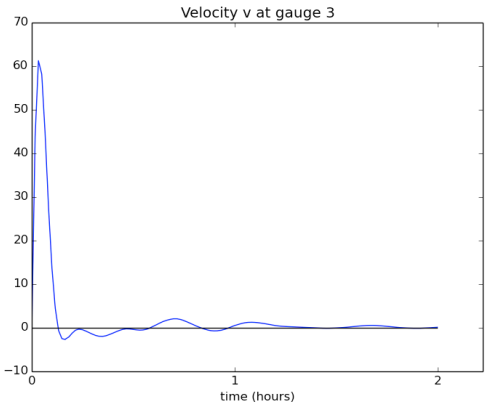
Velocity v at gauge 3
time (hours)

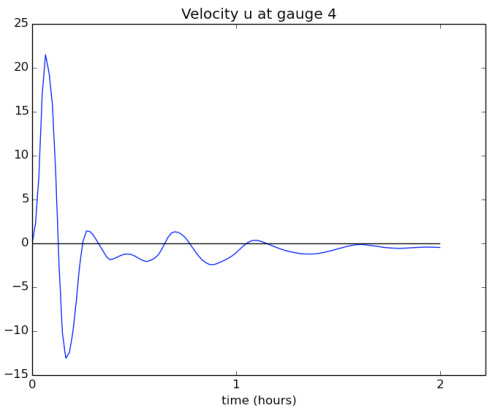
Velocity u at gauge 4
time (hours)

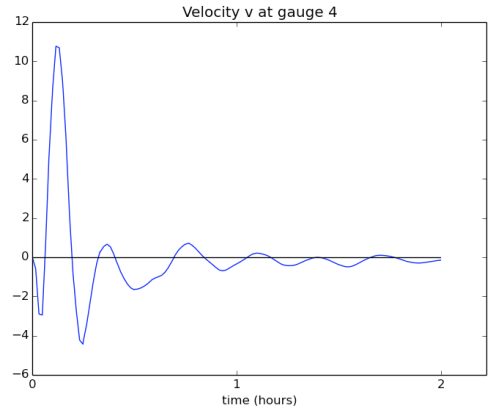
Velocity v at gauge 4
time (hours)

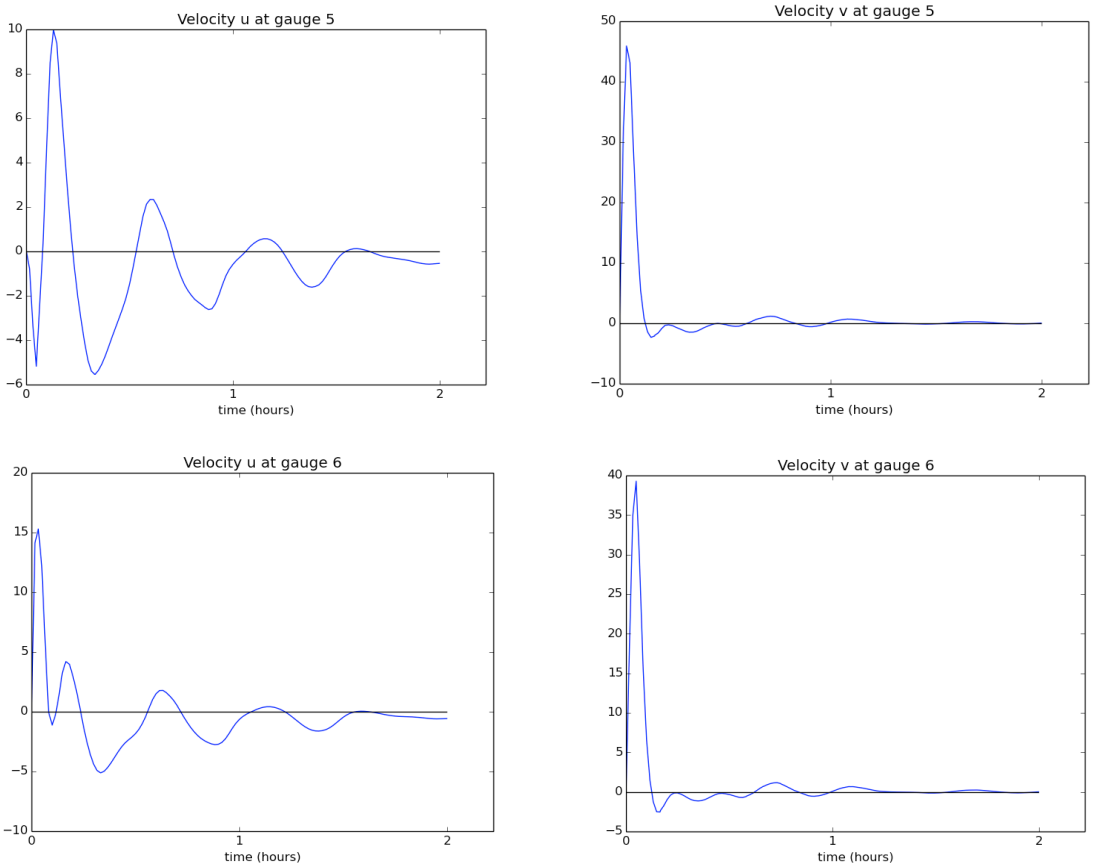

Figure 5: Flow velocities (m/s) computed with the Geoclaw package for gauges 2, 3, 4, 5 and 6.

3.2 The ground motion modeling for the KDB Scenario (Algiers region)

The KDB earthquake shaking maps were produced from the OpenSHA application for a single point rupture that represents the hypocenter off NW of Algiers. The results here presented indicate the level of the peak ground accelerations and the peak ground velocities. Both type of data help to evaluate the areas prone to infrastructure damage along the bay of Algiers and the bay of Bou Ismail and the coastal risk related to the earthquake. The ground shaking levels for the Algiers region shows the dependency on the earthquake location.

The peak ground accelerations (PGA) are shown in the figure 6. The results indicate the highest PGA values are 0.4g – 0.5 g (or 3.924 m/s^2 – 4.905 m/s^2). These are obtained for the western part of the bay of Algiers. The lowest values are simulated for the western part of the Bou Ismail bay (less than 0.15 g, or 1.47 m/s^2). The ground motion modeling indicates the highest seismic risk for an earthquake located off Algiers (2.98E, 36.98N) is for the Algiers Massif (Figure 6). The figure 7 represents the peak ground velocities (PGV) simulated for the same scenario. The highest values for the PGV are distributed in the Algiers Massif (between 35 to 50 cm/sec.). Along the Algiers bay, the values range between 28 to 37 cm/sec. Along the Bou Ismail bay, the velocities are lower and are less than 22 cm/s.

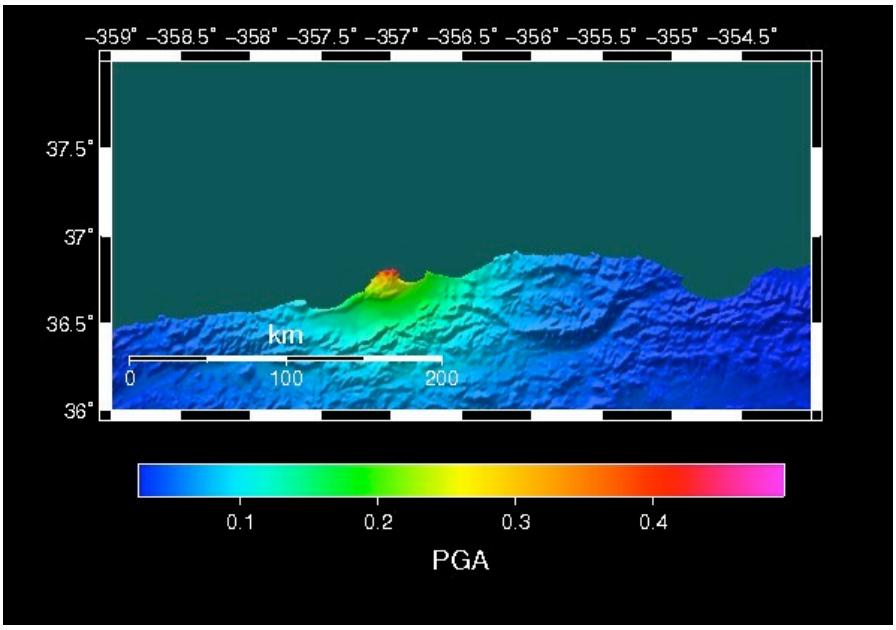

Figure 6: Peak Ground Accelerations (g) simulated for a 7.5 earthquake off Algiers region with the OpenSha application

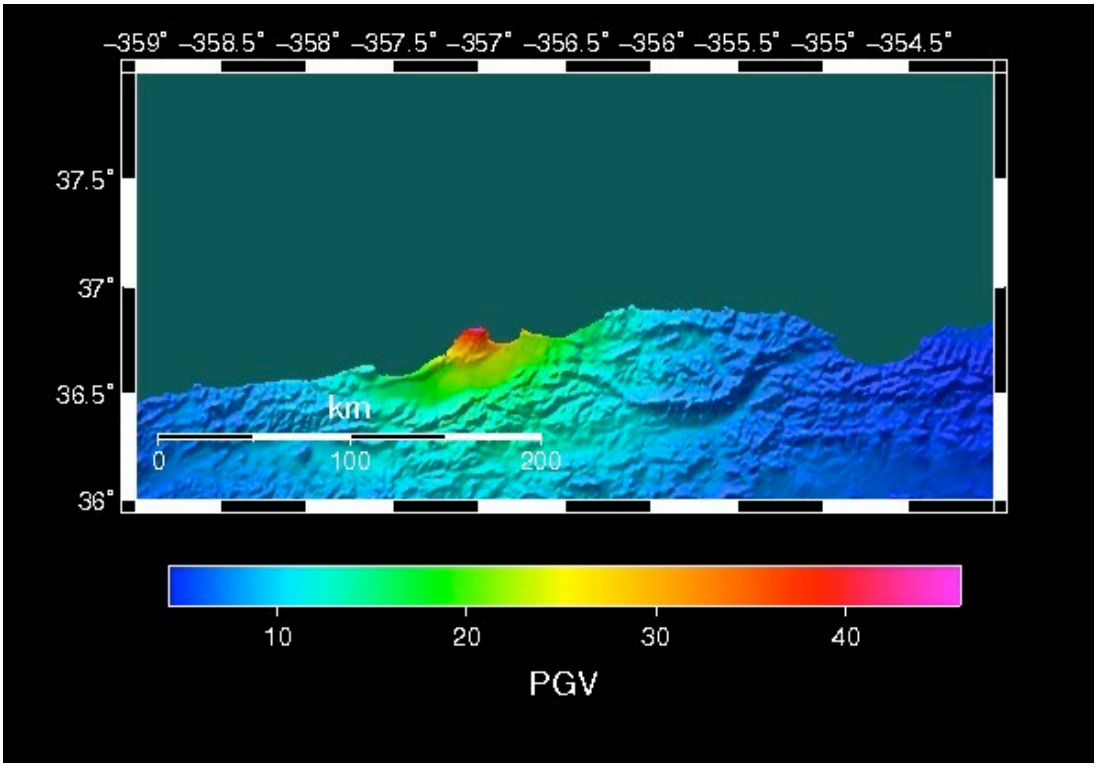

Figure 7: Peak Ground Velocities (cm/sec) simulated for a 7.5 earthquake off Algiers region with the OpenSha application.

Digital Image Processing in the Algiers Bay

Evaluations of LANDSAT and RapidEye imageries clearly show nearly circular currents in the Bay of Algiers. This is visible on the LANDSAT scenes in Figure 8 and the RapidEye scene in Figure 9.

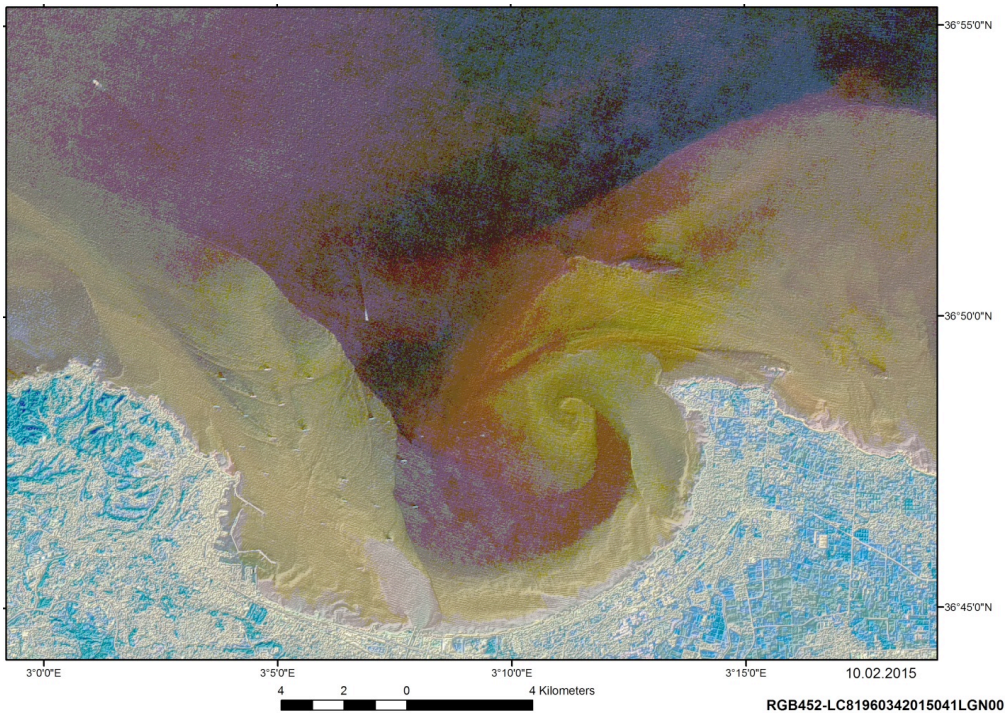

Figure 8: LANDSAT scenes in the Algiers bay

This is visible on the LANDSAT scenes in Figure 8 and the RapidEye scene in Figure 9.

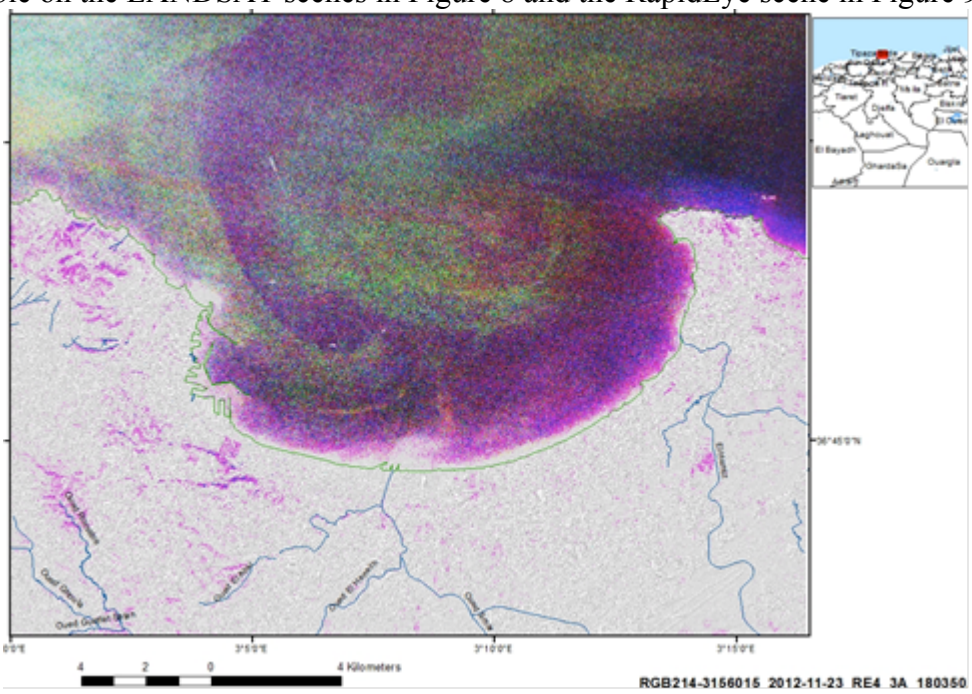

Figure 9: RapidEye scene in the Algiers bay

The development of the nearly circular shaped Bay of Algiers could be explained by such circular streaming dynamics of the water with the consequence of erosional effects. The sea surface-streaming pattern as visible on the Landsat- and RapidEye-scenes of the Bay of Algiers (visualizing the situation only of the upper centimeters) is mainly influenced by the wind situation at the acquisition time, further on by the tidal situation and the input of river water. In case of stronger tsunami events with several tsunami wave fronts circular currents cannot be excluded to occur in the Bay of Algiers as well and, thus, amplify the intensities by interfering and superimposing of incoming waves. The direction and angle of incoming, high energetic flood waves will have a great influence on the currents and dynamics. River mouths are forming an entrance for intruding water waves from the sea. Therefore, even in longer distances from the seaside flooding might be possible affecting the city area of Algiers.

The Figure 10 presents the results of the weighted overlay based on morphometric, causal factors in the area of Algiers showing those areas susceptible to flooding due to the aggregation of causal, morphometric factors. The ASTER DEM derived drainage pattern and the weighted overlay results, presented together with the sealed areas of Algiers contribute to a better visualization of urban areas susceptible to flooding (Figure 10).

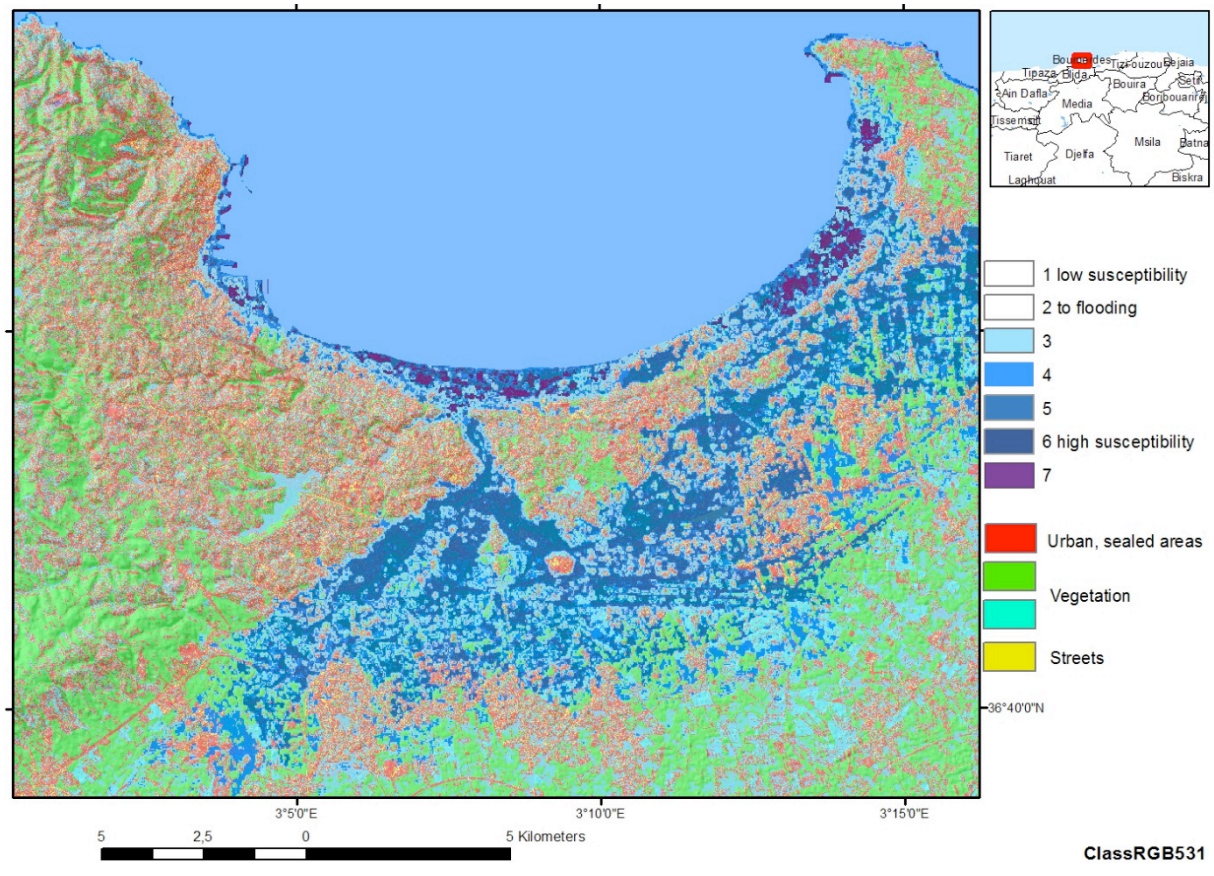

Figure 10: Results of the weighted overlay based on morphometric, causal factors in the area of Algiers

4. DISCUSSION

The purpose of this work was to test a worst-case scenario for an offshore seismogenic structure in the central part of North Algeria. The Khayr Al Din Bank and its related reverse fault system is a serious threat for seismic and tsunami hazard and risk in the coast of Algeria. Seismic shaking maps were computed and tsunami waves were simulated for a 7.5 earthquake off Algiers (Epicenter: 2.98E, 36.98N). The OpenSHA application was used to calculate the peak ground accelerations (PGA) and the peak ground velocities (PGV). The results obtained show the Algiers Massif is the most exposed region as for the seismic risk. The tsunami waves triggered from the 7.56 magnitude off Algiers reach about 1.9 meters in height in the eastern part of the Bou Ismail bay.

Areas exposed to flooding in the coastal zones of Northern-Algeria detected from remote sensing and GIS were also here present. From LANDSAT imageries and weighting tools in the GIS application, a susceptibility to flooding map was constructed / elaborated based on causal, morphometric and triggering factors for the Algiers bay. The highest susceptibility flooding levels are located in the central and eastern part of the Algiers bay.

Assessing a coastal risk from combining the Shindo Scale for earthquakes and the Papadopoulos-Imamura Scale for the tsunamis help to associate physical measurements and data (PGA, water height and flood extent) with observed impact such as (1) the damage on the infrastructure and buildings relatively to the materials used for the constructions (wooden houses, concrete, reinforced concrete, masonry, etc.) and (2) the potential effect on lifeline (Epstein, 2011; Amir et al. 2013). Both scales were used to define a new tsunami risk scale based on a tsunamigenic earthquake vulnerability index (Amir et al., 2013). The results here obtained could be used to assess a rank considering the PGA values and the tsunami velocities for the Bou Ismail bay and the Algiers bay. For that purpose, this study must be completed by additional parameters such as the liquefaction and the rockslide potential, the structural class vulnerability and the available space to evacuate for several points of interest along both bays.

5. CONCLUSION

Coastal cities and exposed communities face various sources of hazards that can impact their livelihoods. In this paper, an interdisciplinary approach was presented to discuss on the coastal risk in the Algiers region known to be a seismogenic zone. Northern Algeria is subjected to tsunami hazard and the Khair Al Din Bank and its related reverse fault are candidates for a worst-case scenario for the Algiers region. A tsunami modeling was then computed using the GeoClaw package for a 7.6 earthquake off Algiers. The surface heights and the flow velocities estimated for several points of interest near and in the coast highlight the threat coastal harbors and cities will face as for structural damage and flooding. Seismic hazard maps were as well generated using the Opensha application for ground motion modeling. The peak ground accelerations and the peak ground velocities data computed for a 7.5 earthquake off Algiers in the Khair Al Din Structure show the Algiers massif is the most exposed to structural damage. Finally, remote sensing is widely used for risk assessment and can be applied to identify locations prone to damage. The water current dynamics and the coastal morphology revealed by satellite imageries were examined

and considered to produce a GIS – map showing areas susceptible to flooding in the Algiers bay. At length, the combination of these three methods converges to same results and conclusions as for areas at risk either due to the earthquake event or the induced tsunami and its related flooding hazard.

REFERENCES

Abrahamson, N. A., & Silva, W. J. (1997). Empirical response spectral attenuation relations for shallow crustal earthquakes. *Seismological Research Letters, 68*(1), 94-127.

Amante, C., & Eakins, B. (2009). *ETOPO 1 Arc-Minute Global Relief Model : Procedures, Data Sources and Analysis* . NOAA Technical Memorandum NESDIS NDGC-24.

Amir, L. A., Cisternas, A., Dudley, W., McAdoo, B. G., & Pararas-Carayanis, G. (2013). A new tsunami risk scale for warning systems - Application to the bay of Algiers (Algeria, Western Mediterranean). *Science of Tsunami Hazards, 32*(2), 116-121.

Amir, L., Cisternas, A., Dudley, W., McAdoo, B. G., & Pararas-Carayannis, G. (2013). A new tsunami risk scale for warning systems - Application to the bay of Algiers (Algeria, West Mediterranean). *Science of Tsunami Hazards, 32*(2), 116-131.

Domzig, A., Yelles, K., Le Roy, C., Deverchere, J., Bouillin, J.-P., Bracene, R., . . . Pauc, H. (2006). Searching for the Africa-Eurasia Miocene boundary offshore western Algeria (MARADJA'03 cruise). *Comptes Rendus Geosciences, 338*(1-2), 80-91.

Epstein, W. (2011). *A Probabilistic Risk Assessment Practioner looks at the Great East Japan Earthquake and Tsunami.* Tokyo: Tokyo Institute of Technology, Ninokata Laboratory.

Field, E. H., EERI, M., Seligson, H. H., Gupta, N., Gupta, V., Jordan, T. H., & Campbell, K. W. (2005). Loss Estimates for a Puente Hills Blind-Thrust Earthquake in Los Angeles, California. *Earthquake Spectra, 21*(2), 329-338.

Field, E. H., Gupta, V., Gupta, N., Maechling, P., & Jordan, T. H. (2005). Hazard Map Calculations Using Grid Computing. *Seismological Research Letters, 76*(5), 565-573.

Field, E. H., Jordan, T. H., & Cornell, C. A. (2003). OpenSHA: A developing community-modeling environment for seismic hazard analysis. *Seismological Research Letters, 74*, 406-4019.

George, D. L., & Leveque, R. J. (2006). Finite Volume Methods and Adaptative Refinement For Global Tsunami Propagation and Local Inundation. *Science of Tsunami Hazards, 24*(5), 326-328.

Heddar, A., Authemayou, C., Djellit, H., Yelles, A., Deverchere, J., Gharbi, S., . . . Van Vliet Lanoe, B. (2012). Preliminary results of a paleoseismological analysis along the Sahel fault (Algeria): New evidence for historical seismic events. *Quaternary International*, 1-14.

Maouche, S., Morhange, C., & Meghraoui, M. (2009). Large boulder accumulation on the Algerian coast evidence tsunami events in the western Mediterranean. *Marine Geology, 262*, 96-104.

Nandasena, N., & Tanaka, N. (2013). *Boulder transport by high-energy (tsunamis): Model development for threshold entrainment and transport.* Research Report, Department of Civil and Environmental Engineering, Saitama Univ.

Okada, Y. (1992). Internal Deformation due to Shear and Tensile Faults in a Half-Space. *Bull. Seism. Soc. Am.*, 82, 1018-1040.

Theilen-Willige, B. (2014). Flooding Hazard in Northern Algeria : Contribution of remote sensing and GIS methods to the detection of areas exposed to flooding in the coastal zones of Northern Algeria. *ICT-DM 2014*, (pp. 1-4). Algiers, Algeria.

Yelles, A., Domzig, A., Deverchere, J., Bracene, R., Mercier de Lepinay, B., Strzerynski, P., . . . Djellit, H. (2009). Plio-Quaternary reactivation of the Neogene margin off NW Algiers, Algeria : The Khayr al Din bank. *Tectonophysics, 475*, 98-116.

Yelles-Chaouche, A. (1991). Coastal Algerian Earthquakes : a potential risk of tsunamis in western Mediterranean ? Preliminary investigation. *Science of Tsunami Hazards, 9*, 47-54.

Yielding, G. (1985). Control of rupture by fault geometry during the 1980 El Asnam (Algeria) earthquake. *Geophys. J. R. astr. Soc., 81*, 641-670.